Nanoscale Advances

ROYAL SOCIETY OF CHEMISTRY

PAPER

View Article Online
View Journal

Cite this: DOI: 10.1039/d5na00897b

Synthesizing porous nanospheres with highly efficient drug loading and sustained release through a thermal-controlled continuous stirred-tank reactor cascade

Huiyu Chen, †[a] Aniket Pradip Udepurkar, †[ab] Christian Clasen, [c] Victor Sebastián Cabeza [defg] and Simon Kuhn *[a]

Received 19th September 2025
Accepted 22nd December 2025

DOI: 10.1039/d5na00897b

rsc.li/nanoscale-advances

Nanospheres hold great promise for drug delivery but face challenges in achieving both high drug loading and sustained release. Here, we present a novel approach to produce porous cyclosporin A-loaded poly(lactic-*co*-glycolic acid) (PLGA) nanospheres *via* a thermal-controlled continuous stirred-tank reactor (CSTR) cascade, featuring rapid solidification of nanoemulsion droplets. This process traps more drug molecules in the nanosphere core by limiting their diffusion towards the surface and surrounding medium, resulting in a core-loaded structure. The resulting PLGA nanospheres exhibit a high cyclosporin A loading capacity and enable sustained drug release through the hydrolytic degradation of the PLGA matrix. Moreover, the total synthesis time is reduced from several hours to 40 min. The CSTR assisted manufacturing approach offers an efficient route for engineering nanospheres with high drug payloads and improved release kinetics, with broad potential for nanomedicine manufacturing.

Introduction

Drug-loaded nanospheres represent a powerful strategy for delivering active pharmaceutical ingredients using inert nanoscale carriers. These nanospheres can protect drug molecules from degradation and promote their transport across biological barriers to reach a target site.[1–4] The inert materials, such as biodegradable polymers, enable sustained drug release, thus allowing for tailored pharmacokinetic properties and reducing the need for repeated dosing.[5,6] Moreover, increasing the drug load per nanosphere allows higher doses per injection, improving patient compliance and minimizing excipient-related side effects.[7–9] For many treatments, achieving a high therapeutic mass fraction is a prerequisite due to strict volume limits on injectable formulations (0.1 mL intradermal, 1 mL subcutaneous, and 1–3 mL intramuscular).[10] These constraints make the development of nanospheres with high drug content critically important.

Engineering high drug-loaded nanospheres is challenging due to inherent limitations arising from their high surface-to-volume ratio. Drugs positioned on the particle surface are susceptible to loss during the formulation and post-formulation processes.[11–13] Nanospheres are primarily composed of non-therapeutic scaffold polymers, such as poly(lactic-*co*-glycolic acid) (PLGA). Drug loadings in most reported studies are lower than 4%; some are even substantially below 1%.[11,14–27] Various strategies have been developed to improve drug loading efficiency through strengthening drug–carrier interactions, such as donor–receptor coordination and covalent conjugation.[28–31] However, these approaches are limited, as they require both the drug and carrier molecules to have specific structural and chemical properties.

Encapsulating a larger fraction of drug molecules within the nanosphere core, rather than leaving a significant portion on the surface, helps overcome surface-to-volume ratio constraints and enhances overall drug loading. This strategy eliminates the dependence on specific molecular features of the drug and carrier. A core-loaded nanosphere structure not only increases the total drug content but also offers better control over the drug release. Drug release from nanospheres occurs in two phases: an initial burst release caused by the rapid diffusion of surface-located drugs, followed by a more sustained release through

[a]*Department of Chemical Engineering, Process Engineering for Sustainable Systems (ProcESS), KU Leuven, Celestijnenlaan 200F, Leuven 3001, Belgium. E-mail: simon.kuhn@kuleuven.be*

[b]*Department of Chemical Engineering, Massachusetts Institute of Technology, 77 Massachusetts Avenue, Cambridge, MA 02139, USA*

[c]*Department of Chemical Engineering, Soft Matter, Rheology and Technology (SMaRT), KU Leuven, Celestijnenlaan 200J, Leuven 3001, Belgium*

[d]*Instituto de Nanociencia y Materiales de Aragón (INMA), CSIC-Universidad de Zaragoza, Zaragoza 50009, Spain*

[e]*Department of Chemical and Environmental Engineering Universidad de Zaragoza Campus Rio Ebro, 50018 Zaragoza, Spain*

[f]*Laboratorio de Microscopías Avanzadas, Universidad de Zaragoza, 50018 Zaragoza, Spain*

[g]*Networking Research Center on Bioengineering, Biomaterials and Nanomedicine (CIBER-BBN), 28029 Madrid, Spain*

† These authors contributed equally to this work.

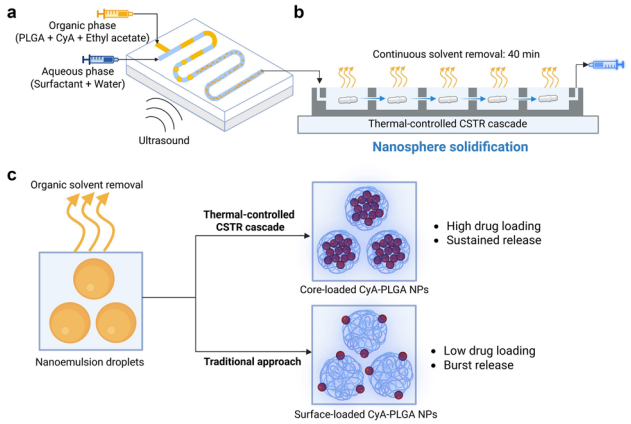

Fig. 1 Synthesis process of cyclosporin A-loaded PLGA nanospheres (CyA-PLGA NPs). The setup consists of (a) an ultrasonic microreactor for emulsion generation and (b) a continuous thermal-controlled CSTR cascade for solvent removal and nanosphere solidification. (c) Solvent removal and solidification processes at the droplet/particle level, along with the resulting nanosphere properties, compared to the traditional batch approach. The illustration was created with Biorender.com.

the hydrolytic degradation of the PLGA matrix.[32–34] By increasing the amount of drug loaded in the core, the initial burst release and resulting toxicity risks can be reduced, leading to a more sustained and prolonged release profile. Nanospheres could be formed from nanoemulsion droplets as the organic solvent evaporates (Fig. 1c), leading us to reasonably hypothesize that the solvent removal process would play a critical role in determining the solidification of drug and polymer molecules. By optimizing this process, it may be possible to fabricate core-loaded nanospheres with high drug loading and improved release kinetics.

For continuous nanosphere synthesis, microfluidic nanoprecipitation is used in many studies.[6,35–38] Although this technique can produce ultra-small nanospheres ranging from 20 to 100 nm, it struggles with a low drug loading capacity (<4%).[14,39–41] Increasing the particle size can improve drug loading, but it will compromise the ability to cross biological barriers. This hinders particular applications like brain-targeted delivery, which requires particles to be below 100 nm to cross the blood–brain barrier.[42–44] Furthermore, the small channel sizes required for rapid mixing in microfluidics can lead to issues like low throughput and microchannel clogging.[45–47]

Another commonly used synthesis method is emulsion-solvent evaporation. In 2007, Budhian *et al.*[20] attempted to increase drug loading by adjusting the pH during solvent evaporation to reduce drug diffusion into the aqueous phase. However, they achieved a maximum drug loading of 2.5%. In 2016, de Solorzano *et al.*[48] used microchannel emulsification for high-throughput synthesis (~10 g h^{-1}) of cyclosporin A-loaded PLGA nanospheres. However, the resulting particles had a mean size far exceeding 200 nm. Recently, Operti *et al.*[49] introduced an inline sonicator for continuous emulsification, but the solvent evaporation was performed in a batch mode with dilution and stirring for 1 hour, and the smallest mean particle size achieved was 184.7 nm. To conclude, the synthesis of drug-loaded PLGA nanospheres through emulsion-solvent evaporation has not been fully transitioned to a continuous process. Achieving a mean particle size under 100 nm remains challenging, and the impact of solvent evaporation temperature on drug encapsulation was largely overlooked in previous studies.

In this work, we control the solvent removal process using a continuous stirred-tank reactor (CSTR) cascade (Fig. 1b), which provides thermal regulation, to solidify the drug and polymer molecules. This approach contrasts with previous studies,[48–51] where solvent removal was performed in batch mode and remained largely unoptimized. This continuous manufacturing strategy eliminates batch-to-batch variations and provides a well-defined scale-up pathway,[52,53] addressing two major challenges in the industrialization of nanomedicines.[54–58] To validate our approach, cyclosporin A (CyA) is selected as a model peptide drug due to its poor water solubility and limited bioavailability (class II from the Biopharmaceutical Classification System, BCS). The solvent removal step is systematically optimized, and its impact on particle size distribution, morphology, and drug loading efficiency of cyclosporin A-loaded PLGA nanospheres (CyA-PLGA NPs) is assessed. Furthermore, *in vitro* drug release studies are conducted to evaluate the sustained release profile. Process efficiency and residual solvent content are also analysed to ensure the robustness and scalability of the developed method.

Results and discussion

Synthesis and characterization of CyA-PLGA NPs

CyA-PLGA NPs were synthesized using the emulsion–solvent evaporation technique. In the first step, an automated ultrasonic microreactor was employed to generate nanoemulsion droplets. The organic phase, consisting of PLGA and cyclosporin A dissolved in ethyl acetate, and the aqueous phase, consisting of the surfactant Poloxamer 407 in Milli-Q water, were introduced into the microreactor. Ultrasonic energy was applied *via* a piezoelectric transducer plate attached to the bottom of the reactor to facilitate emulsification (Fig. 1a). Following droplet formation, the nanoemulsion was fed into a CSTR cascade for continuous thermal-controlled solvent removal (Fig. 1b). The outlet of the CSTR cascade was connected to a syringe pump, which continuously withdrew the solidified CyA-PLGA NP suspension. The temperature of the CSTR cascade was regulated using a circulating water jacket located beneath the wells (Fig. 3a). The entire process was automated and conducted at a constant flow rate of 250 μL min^{-1}, with an overall residence time of ~40 min. For comparison, a traditional batch method was carried out by collecting the nanoemulsion from the microreactor outlet into a glass vial (Fig. 3b), followed by magnetic stirring for at least 4 hours at room temperature to allow for solvent evaporation.

For effective drug delivery, nanospheres smaller than 200 nm with a polydispersity index (PDI) below 0.2 are desired,[59,60] while brain-targeted therapies typically demand even smaller sizes—under 100 nm.[42,44,61] To meet these criteria, the emulsification step in the ultrasonic microreactor was systematically optimized (Table S2) before integrating the thermal-controlled

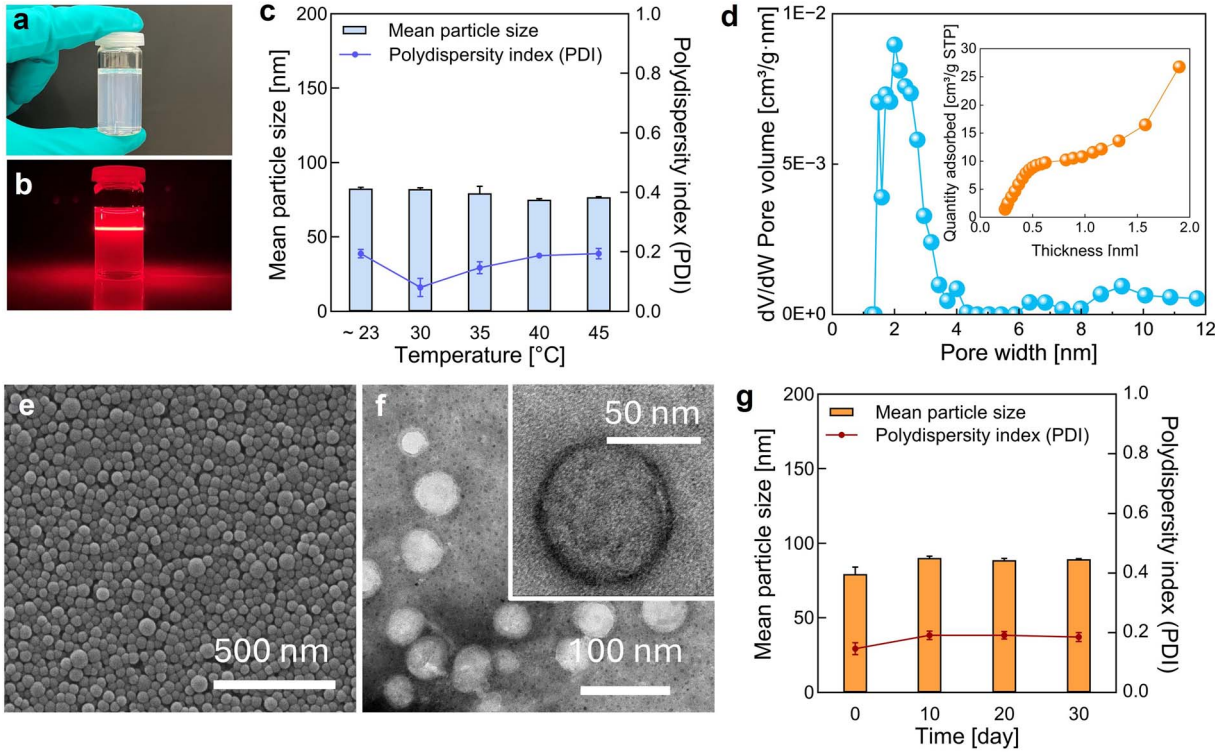

Fig. 2 Characterization of CyA-PLGA NPs. (a) Visual appearance of the CyA-PLGA NP suspension. (b) Tyndall effect observed in the suspension using a laser pointer. (c) Mean particle size and polydispersity index (PDI) measured by dynamic light scattering (DLS). (d) Porosity distribution determined by density functional theory (DFT) analysis and *t*-plot analysis of CyA-PLGA NPs based on Brunauer–Emmett–Teller (BET) isotherms, measured at standard temperature and pressure (STP, 273 K and 101.325 kPa) with N_2. Representative (e) scanning electron microscopy (SEM) image, (f) transmission electron microscopy (TEM) images, and (g) stability profile over 30 days (storage 2–8 °C) of CyA-PLGA NPs prepared *via* the thermal-controlled CSTR cascade at 35 °C. Data are presented as mean ± SD ($n = 3$).

CSTR cascade. After implementing the CSTR cascade for continuous solvent removal, the process temperature was varied from room temperature (~23 °C) to 45 °C. Across this temperature range, the resulting CyA-PLGA NPs consistently maintained a mean particle size below 82 nm and a PDI below 0.2, fulfilling the size distribution requirements for biomedical applications. The pore size distribution results from the Brunauer–Emmett–Teller (BET) analysis (Fig. 2d) indicate the presence of micropores around 1.5 nm and mesopores in the 2–3 nm range. Larger pores (>5 nm) are likely due to interstitial voids between the nanospheres. The coexistence of micropores and mesopores is further confirmed by the *t*-plot curve, which exhibits a characteristic profile typical of micro–mesoporous materials.[62] SEM and TEM images revealed a smooth, spherical morphology with a uniform size distribution. No significant morphological differences were observed between nanoparticles synthesized at ~23 °C (Fig. S10) and at 35 °C (Fig. 2e and f), indicating that the mild thermal treatment does not compromise particle integrity. Additionally, the CyA-PLGA NPs demonstrated good storage stability, retaining their size distribution for at least 30 days when stored at 2–8 °C (Fig. 2g).

Thermal-controlled CSTR cascade for enhanced drug loading

The solvent removal time was significantly reduced from over 4 hours (ref. 63) to just 40 min by replacing the conventional batch method (Fig. 3b) with a continuous CSTR cascade (Fig. 3a), which doubled the surface-to-volume ratio (Table S1). At a fixed duration of 40 min and room temperature (~23 °C), the residual ethyl acetate concentration decreased from 141.3 μL mL^{-1} (batch) to 8.0 μL mL^{-1} (CSTR), demonstrating improved efficiency. However, to meet EMA regulations for Class 3 solvents,[64] which require residual levels below 5 μL mL^{-1} (5000 ppm), faster solvent removal is necessary. This was addressed by introducing thermal control at elevated temperatures.

The residual ethyl acetate content in each CSTR well during solvent removal (Fig. 3c) and in the final nanosphere suspension (Fig. 3d), along with the drug loading (DL, Fig. 3e) and encapsulation efficiency (EE, Fig. 3f) of the resulting CyA-PLGA NPs, was quantified by HPLC. The results showed that at 30 °C and 35 °C the final residual ethyl acetate was significantly reduced to 2.3 ± 0.3 μL mL^{-1} and 0.9 ± 0.3 μL mL^{-1}, respectively, both well below the 5 μL mL^{-1} threshold. Interestingly, a slight increase in residual solvent was observed at 40 °C (1.5 ± 0.4 μL mL^{-1}) and 45 °C (2.4 ± 0.1 μL mL^{-1}). The drug loading increased from 4.2 ± 1.3% at ~23 °C to a peak value of 7.6 ± 0.4% at 35 °C, but then declined to 3.6 ± 0.7% and 3.9 ± 0.3% at 40 °C and 45 °C, respectively, even below the value at room temperature (~23 °C). A similar trend was observed for the encapsulation efficiency, which rose from 26.5 ± 8.5% to 49.0 ± 2.5% at 35 °C and then decreased to 22.7 ± 4.6% and 24.4 ± 2.2% at the higher temperatures.

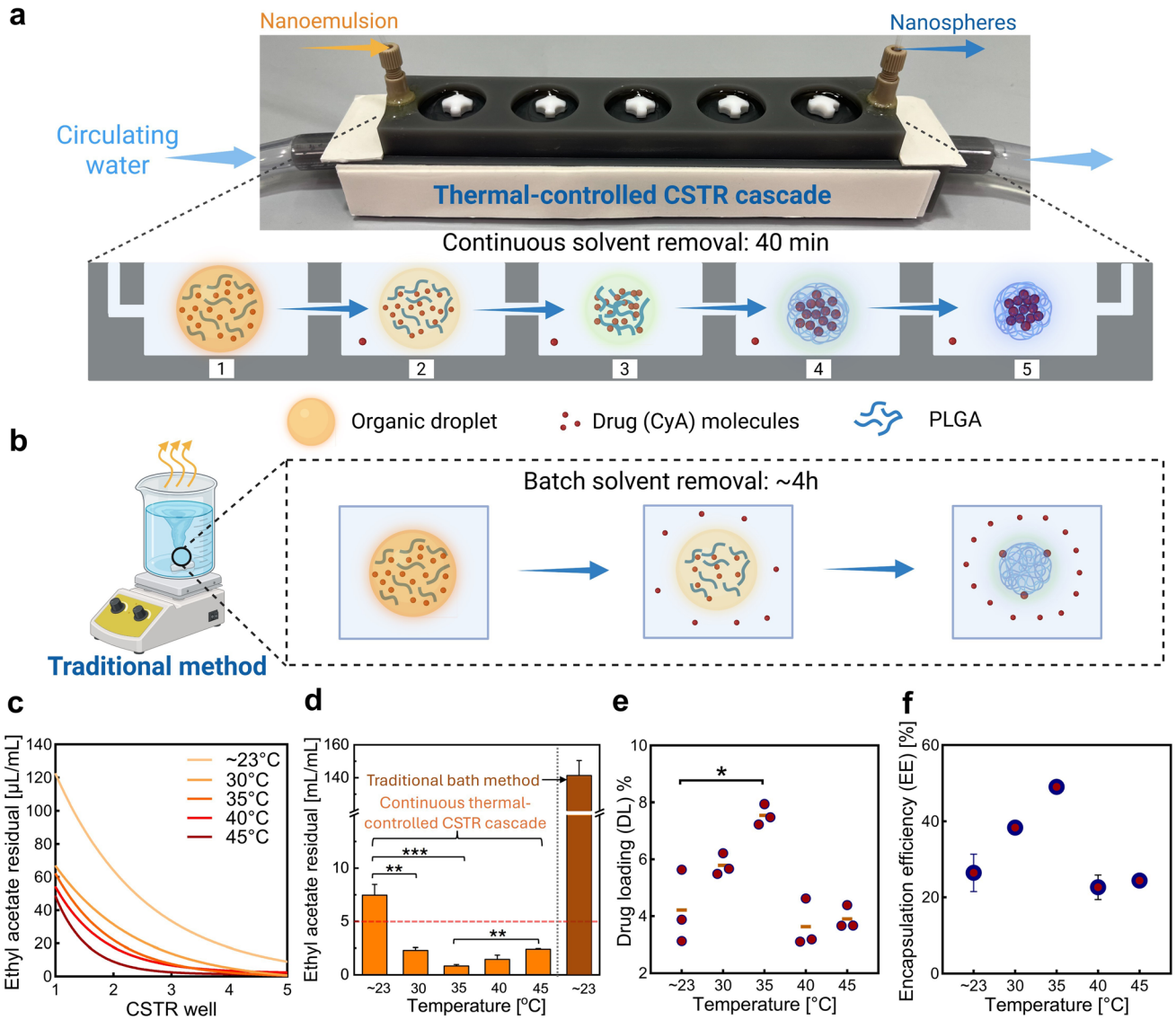

Fig. 3 Optimization of the thermal-controlled CSTR cascade and the resulting enhancement in drug loading efficiency. Schematic comparison of the organic solvent removal and nanoparticle formation process using (a) thermal-controlled CSTR cascade and (b) traditional batch method. (c) Residual ethyl acetate concentrations measured in each CSTR well (1–5) during the solvent removal process. (d) Final residual solvent content in the nanoparticle suspension. (e) Drug loading (DL) and (f) encapsulation efficiency (EE) of the resulting CyA-PLGA NPs obtained at varying CSTR cascade temperatures (~23 °C to 45 °C). In graphic (d), the red dashed line indicates the maximum allowed residual level of ethyl acetate according to EMA guidelines (5 μL mL^{-1}). Data are shown as mean ± SD, $n = 3$. Statistical significance is indicated as *$p < 0.05$, **$p < 0.01$, and ***$p < 0.001$. Only relevant and significant statistical comparisons are highlighted.

The initial reduction in residual ethyl acetate at moderately elevated temperatures is attributed to an accelerated solvent removal rate, as further supported by measurements from individual CSTR wells (1–5) during the process (Fig. 3c). The observed improvement in drug loading efficiency results from more efficient solvent removal achieved through the thermal-controlled CSTR cascade. During this process, the organic solvent must first diffuse from the emulsion droplets into the surrounding aqueous phase before it can evaporate.[65,66] Katou *et al.*[67] proposed a mathematical model to describe the kinetics of this solvent transfer from oil droplets to the aqueous phase:

$$\frac{\partial C_d}{\partial t} = \frac{D}{r^2} \cdot \frac{\partial}{\partial r} \cdot \left(r^2 \cdot \frac{\partial C_d}{\partial r} \right) \quad (1)$$

where C_d stands for the solvent concentration, t stands for time, r stands for radial position, and D stands for the solvent diffusion coefficient. According to the Wilke–Chang equation, the solvent diffusion coefficient D is given by

$$D = \frac{7.4 \times 10^{-8} (\varnothing M)^{1/2} T}{\eta V^{0.6}} \quad (2)$$

where $\varnothing$ is the association parameter, M is the molecular mass of the solvent, T is the temperature, η is the viscosity, and V is the molecular volume. The diffusion coefficient is proportional to the temperature, meaning that at higher temperatures, solvent removal occurs more rapidly. This accelerates droplet solidification and limits the time available for drug diffusion

into the external aqueous phase. As a result, a larger amount of the drug is retained within the polymeric matrix of the nanospheres, significantly enhancing drug loading.

However, at further elevated temperatures of 40 °C and 45 °C—surpassing the glass transition temperature ($T_g^{'}$) of PLGA (Fig. S11)—the polymer does not solidify into a rigid, glassy state but instead transitions into a softer, rubbery phase.[68–70] In this rubbery state, stronger polymer–solvent interactions hinder solvent diffusion and evaporation, resulting in higher residual ethyl acetate levels despite the elevated temperature. Moreover, this rubbery state leads to two major effects: (i) the diffusion of the organic solvent slows down considerably, giving the drug more time to diffuse out of the polymeric matrix and escape into the aqueous phase, reducing drug retention; (ii) in some cases, the polymer–drug mixture fails to solidify into nanoparticles before reaching the liquid surface during evaporation. Instead, it forms a polymeric film on the liquid surface in the CSTR (as observed during experiments), leading to a loss of the drug material and reduced nanoparticle formation. Consequently, the drug loading efficiency at 40 °C and 45 °C declined, even falling below that achieved at room temperature (~23 °C).

Therefore, 35 °C was determined to be the optimal solvent removal temperature in the CSTR cascade, as it enables ideal particle size distribution, maximizes the drug loading efficiency, and minimizes the residual ethyl acetate content, while preventing the detrimental effects of PLGA transitioning into its rubbery state above $T_g^{'}$.

To confirm that these improvements were due to the nature of the thermal-controlled CSTR cascade nanotechnology, rather than temperature alone, a batch solvent removal was also performed at 35 °C for comparison (Table S4). When the batch process was run for the same duration as that of the CSTR cascade (40 min), the drug loading efficiency was extremely low at 0.8 ± 0.1%, indicating that almost no drug was encapsulated. As previously discussed, this is attributed to the poor solvent removal efficiency of the batch method, which left a high residual ethyl acetate concentration (91.9 ± 1.6 μL mL^{-1}). With the aqueous phase nearing saturation, the diffusion of ethyl acetate from the droplets was restricted, significantly slowing solidification. This prolonged diffusion window allowed drug molecules to escape into the aqueous phase before being entrapped. Even after extending the batch evaporation to 4 hours, the drug loading efficiency only modestly increased to 2.5 ± 0.9%, still far below the value achieved with the CSTR cascade. These results confirm that the significant improvement in drug loading was primarily due to the efficient solvent removal enabled by the thermal-controlled CSTR cascade.

In vitro drug release

The release of a poorly water-soluble drug from PLGA nanospheres typically happens in two phases (Fig. 4a). The first phase is a rapid initial burst release, driven by the diffusion of the drug located near the particle surface. The second phase is more sustained and is attributed to the hydrolysis of the PLGA and erosion of the polymeric matrix, which releases the drug encapsulated in the nanosphere core.[32–34] If the enhanced solvent removal rate indeed results in increased drug encapsulation in the nanosphere core, CyA-PLGA NPs synthesized using the thermal-controlled CSTR cascade at 35 °C should exhibit less of an initial burst release and more drug release during the second sustained phase.

To provide a meaningful comparison, we selected the batch solvent evaporation at ~23 °C (Batch @ ~23 °C) to represent the slowest evaporation rate. The drug release profile over 120 h, depicted in Fig. 4b, confirms the hypothesis. During the first 24 hours of the initial release phase, there was no statistically significant difference between the two samples. However, by the end of the burst release phase (72 h), 93% of the drug encapsulated in the Batch @ ~23 °C nanospheres was released, indicating that a major fraction of the CyA molecules was located close to the surface. In contrast, the CSTR @ 35 °C nanospheres only released 76% of their drug content during the initial burst phase (48 h), leaving 24% encapsulated within the nanosphere core for a slower, sustained release. The cumulative drug release gradually declined in the second phase, as the drug continued to be released, but at a slower rate than its degradation, making the net change appear negative. This trend aligns with the CyA stability profile observed in our degradation test (Fig. S9) and is consistent with findings reported in other studies.[71,72]

Next, we conducted an additional *in vitro* drug release study on CyA-PLGA NPs prepared *via* batch solvent evaporation at 35 °C (Batch @ 35 °C). The aim was to assess whether the core-loaded drug distribution observed in nanospheres produced by the CSTR cascade resulted primarily from the high solvent removal efficiency of the thermal-controlled CSTR cascade process, or if similar characteristics could be achieved by applying the same elevated temperature in a conventional batch process. As shown in Fig. 4c, the Batch @ 35 °C nanospheres exhibited a sharp burst release, with 86% of the encapsulated drug released within the very first 9 h. This release was even more abrupt than that of the Batch @ ~23 °C nanospheres, suggesting that the drug was located even closer to the particle surface. By 24 hours, the CyA concentration in the release medium had already begun to decline due to degradation, and the drop was more pronounced because there was little to no sustained release between 9 and 24 hours to replenish the drug. In the end, the sustained release phase began after 48 h, corresponding to the release of the remaining 14% of the drug from the nanosphere core.

Based on the drug release results, we can conclude that the Batch @ 35 °C nanospheres contained a larger fraction of the drug encapsulated in the core (14%) compared to the Batch @ ~23 °C nanospheres (7%), but still less than the CSTR @ 35 °C nanospheres (24%). This suggests that the elevated temperature enhanced solvent diffusion from the droplets into the aqueous phase, allowing more drug to be retained in the nanoparticle core. However, the batch process is limited by a low surface-to-volume ratio, making the evaporation of solvent from the aqueous phase into air the rate-limiting step. This inefficiency resulted in a high residual solvent concentration in the aqueous phase, which in turn suppressed further diffusion of organic

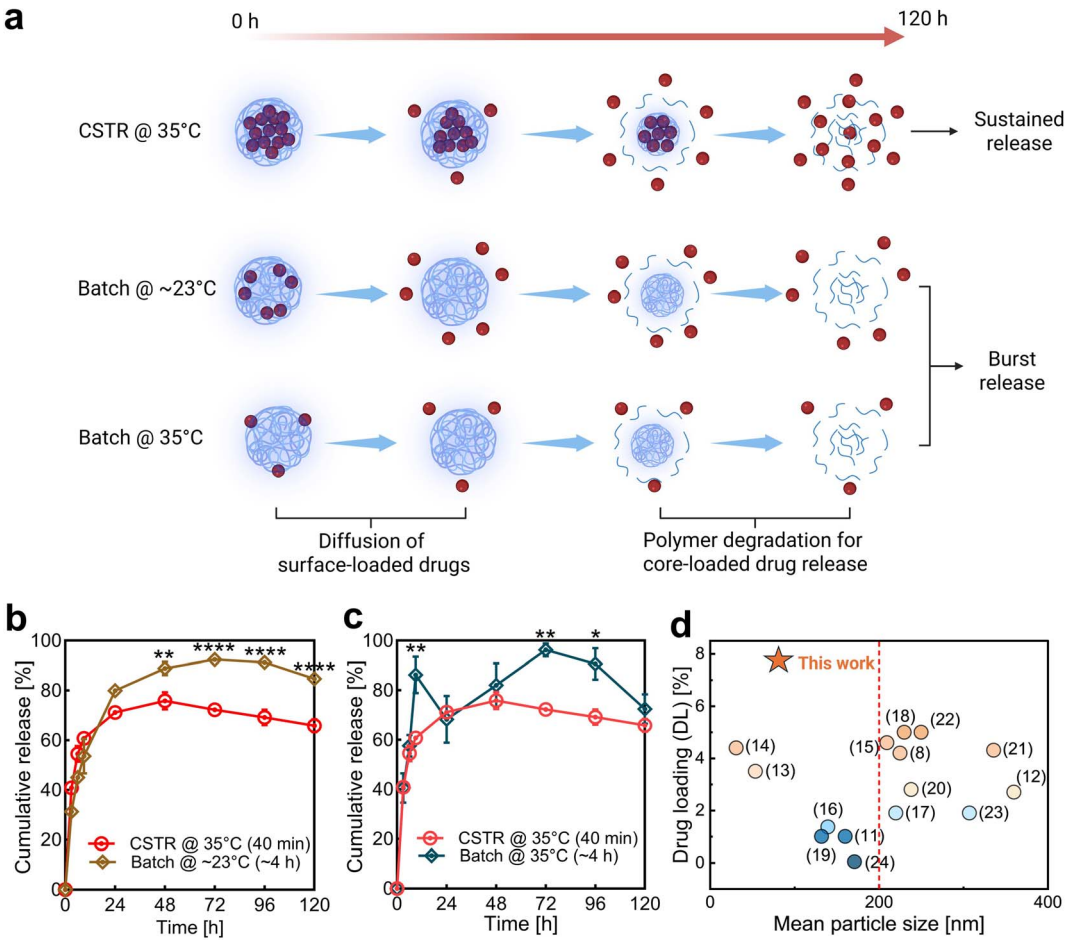

Fig. 4 *In vitro* drug release demonstrating the advantage of the core-loaded nanoparticle structure. (a) Schematic illustration of the two-phase drug release mechanism from PLGA nanoparticles. Sustained and burst release profiles resulting from core-loaded and surface-loaded drug distributions, respectively. (b and c) *In vitro* drug release data of CyA-PLGA NPs prepared *via* the thermal-controlled CSTR cascade at 35 °C (CSTR @ 35 °C), compared to those prepared using the traditional batch method at room temperature (Batch @ ~23 °C) and at 35 °C (Batch @ 35 °C). Data are presented as mean ± SD ($n = 3$). Statistical significance is indicated as follows: *$P < 0.05$; **$P < 0.01$; ***$P < 0.001$; ****$P < 0.0001$. (d) Positioning our core-loaded CyA-PLGA NPs within the landscape of benchmark studies,[11,14–27] highlighting their exceptional ability to simultaneously achieve both a high drug loading efficiency and a small particle size (two critical and often mutually exclusive parameters in nanoparticle synthesis). The red dashed line in panel (d) marks the <200 nm threshold typically considered suitable for drug delivery applications.

solvent from the droplets. Consequently, solvent accumulated at the droplet/nanoparticle interface, providing more time for drug molecules to diffuse into the aqueous phase and be lost, leading to lower drug loading efficiency (2.5 ± 0.9%) compared to the CSTR @ 35 °C (7.6 ± 0.4%). Moreover, this solvent accumulation forces a larger portion of the drug toward the sphere surface, as evidenced by a rapid burst release of 86% of the drug within the first 9 h, in contrast to the slower burst release observed in Batch @ ~23 °C nanospheres (93% released over 48 h). Therefore, the improvement was not solely due to the elevated temperature, but was primarily driven by the high solvent removal efficiency achieved through the thermal-controlled CSTR cascade.

Conclusions

In summary, we have developed a thermal-controlled CSTR cascade nanotechnology for the synthesis of CyA-PLGA NPs, achieving a significantly improved drug loading efficiency and a more sustained release profile. The formation of nanospheres with high drug loading is a result of a larger fraction of drug molecules solidifying at the particle core, realized by a more efficient solvent removal in the CSTR cascade at 35 °C. The achieved drug loading is, to our knowledge, the highest reported for sub-100 nm CyA-PLGA NPs, significantly exceeding the previously reported maximum of 4.6%[11,14–27] (Fig. 4d). The core-loaded structure not only provides a higher drug payload, but also enables gradual release of drug molecules. The sustained release from high drug-loaded nanospheres may contribute to an enhanced therapeutic efficacy and reduced adverse effects for drug delivery applications. Additionally, the robustness and scalability of the thermal-controlled CSTR cascade provide a promising pathway for clinical translation, aligning with FDA guidelines for modern pharmaceutical manufacturing.[73]

Author contributions

Conceptualization: H. C., A. P. U. and V. S. C. Methodology: H. C., A. P. U. and V. S. C. Experiments: H. C., A. P. U., and V. S. C. Writing – original draft: H. C. and A. P. U. Writing – review and editing: C. C., V. S. C., and S. K. Data curation: H. C. and A. P. U. Supervision: C. C., V. S. C., and S. K. Funding acquisition: S. K.

Conflicts of interest

There are no conflicts to declare.

Data availability

Supplementary information (SI): materials and methods, supplementary results of nanosphere synthesis, images, degradation studies, and numerical data corresponding to the plotted figures. See DOI: https://doi.org/10.1039/d5na00897b.

Acknowledgements

Financial support from the Research Foundation FLANDERS (G0B5921N and G088922N) is acknowledged. V. S. C. acknowledges support from the Spanish Ministry of Science and Innovation (grant PID2021-127847OB-I00), the NextGenerationEU/PRTR project (PDC2022-133866-I00), CIBER-BBN, ELECMI and NANBIOSIS ICTSs. H. C. acknowledges FWO Flanders for a strategic basic PhD fellowship (1S06425N). The authors also thank Lisa De Vriendt and Elena Brozzi for their assistance with the DSC measurements; Keiran Mc Carogher and Lorijn De Vrieze for their support in constructing the experimental setup; Prof. Erin Koos and Yanshen Zhu for providing access to and guidance with the DLS measurements; and Pieter Adriaenssens for his help with the HPLC analysis.

References

1 E. Blanco, H. Shen and M. Ferrari, Principles of Nanoparticle Design for Overcoming Biological Barriers to Drug Delivery, *Nat. Biotechnol.*, 2015, 941–951, DOI: 10.1038/nbt.3330.

2 M. R. Chiang, C. W. Hsu, W. C. Pan, N. T. Tran, Y. S. Lee, W. H. Chiang, Y. C. Liu, Y. W. Chen, S. H. Chiou and S. H. Hu, Reprogramming Dysfunctional Dendritic Cells by a Versatile Catalytic Dual Oxide Antigen-Captured Nanosponge for Remotely Enhancing Lung Metastasis Immunotherapy, *ACS Nano*, 2025, **19**(2), 2117–2135, DOI: 10.1021/acsnano.4c09525.

3 T. M. H. Huynh, P. X. Huang, K. L. Wang, N. T. Tran, H. M. Iao, W. C. Pan, Y. H. Chang, H. W. Lien, A. Y. L. Lee, T. C. Chou, W. H. Chiang and S. H. Hu, Reprogramming Immunodeficiency in Lung Metastases *via* PD-L1 SiRNA Delivery and Antigen Capture of Nanosponge-Mediated Dendritic Cell Modulation, *ACS Nano*, 2025, **19**(27), 25134–25153, DOI: 10.1021/acsnano.5c05395.

4 B. N. Yalamandala, Y. J. Chen, Y. H. Lin, T. M. H. Huynh, W. H. Chiang, T. C. Chou, H. W. Liu, C. C. Huang, Y. J. Lu, C. S. Chiang, L. A. Chu and S. H. Hu, A Self-Cascade Penetrating Brain Tumor Immunotherapy Mediated by Near-Infrared II Cell Membrane-Disrupting Nanoflakes *via* Detained Dendritic Cells, *ACS Nano*, 2024, **18**(28), 18712–18728, DOI: 10.1021/acsnano.4c06183.

5 N. C. Brigham, R. R. Ji and M. L. Becker, Degradable Polymeric Vehicles for Postoperative Pain Management, *Nat. Commun.*, 2021, **12**, 1367, DOI: 10.1038/s41467-021-21438-3.

6 D. Liu, H. Zhang, F. Fontana, J. T. Hirvonen and H. A. Santos, Microfluidic-Assisted Fabrication of Carriers for Controlled Drug Delivery, *Lab Chip*, 2017, 1856–1883, DOI: 10.1039/c7lc00242d.

7 S. Shen, Y. Wu, Y. Liu and D. Wu, High Drug-Loading Nanomedicines: Progress, Current Status, and Prospects, *Int. J. Nanomed.*, 2017, 4085–4109, DOI: 10.2147/IJN.S132780.

8 J. Della Rocca, D. Liu and W. Lin, Are High Drug Loading Nanoparticles the next Step Forward for Chemotherapy?, *Nanomedicine*, 2012, 303–305, DOI: 10.2217/nnm.11.191.

9 W. Chen, S. Zhou, L. Ge, W. Wu and X. Jiang, Translatable High Drug Loading Drug Delivery Systems Based on Biocompatible Polymer Nanocarriers, *Biomacromolecules*, 2018, 1732–1745, DOI: 10.1021/acs.biomac.8b00218.

10 S. Sienkiewicz, and J. Palmunen, *Clinical Nursing Calculations*, Jones & Bartlett Learning, 2015.

11 T. Govender, S. Stolnik, M. C. Garnett, L. Illum and S. S. Davis, PLGA Nanoparticles Prepared by Nanoprecipitation: Drug Loading and Release Studies of a Water Soluble Drug, *J. Controlled Release*, 1999, **57**(2), 171–185, DOI: 10.1016/S0168-3659(98)00116-3.

12 S. F. Chin, F. B. Jimmy and S. C. Pang, Size Controlled Fabrication of Cellulose Nanoparticles for Drug Delivery Applications, *J. Drug Delivery Sci. Technol.*, 2018, **43**, 262–266, DOI: 10.1016/j.jddst.2017.10.021.

13 C. Rodrigues de Azevedo, M. von Stosch, M. S. Costa, A. M. Ramos, M. M. Cardoso, F. Danhier, V. Préat and R. Oliveira, Modeling of the Burst Release from PLGA Micro- and Nanoparticles as Function of Physicochemical Parameters and Formulation Characteristics, *Int. J. Pharm.*, 2017, **532**(1), 229–240, DOI: 10.1016/J.IJPHARM.2017.08.118.

14 B. Todaro, A. Moscardini and S. Luin, Pioglitazone-Loaded PLGA Nanoparticles: Towards the Most Reliable Synthesis Method, *Int. J. Mol. Sci.*, 2022, **23**(5), 2522, DOI: 10.3390/ijms23052522.

15 J. Cheng, B. A. Teply, I. Sherifi, J. Sung, G. Luther, F. X. Gu, E. Levy-Nissenbaum, A. F. Radovic-Moreno, R. Langer and O. C. Farokhzad, Formulation of Functionalized PLGA-PEG Nanoparticles for *in vivo* Targeted Drug Delivery, *Biomaterials*, 2007, **28**(5), 869–876, DOI: 10.1016/j.biomaterials.2006.09.047.

16 W. S. Cheow and K. Hadinoto, Factors Affecting Drug Encapsulation and Stability of Lipid-Polymer Hybrid Nanoparticles, *Colloids Surf., B*, 2011, **85**(2), 214–220, DOI: 10.1016/j.colsurfb.2011.02.033.

17 C. Zhang, Y. Cheng, D. Liu, M. Liu, H. Cui, B. Zhang, Q. Mei and S. Zhou, Mitochondria-Targeted Cyclosporin A Delivery System to Treat Myocardial Ischemia Reperfusion Injury of

Rats, *J. Nanobiotechnol.*, 2019, **17**, 18, DOI: 10.1186/s12951-019-0451-9.

18 I. Takeuchi, A. Kagawa and K. Makino, Skin Permeability and Transdermal Delivery Route of 30-nm Cyclosporin A-Loaded Nanoparticles Using PLGA-PEG-PLGA Triblock Copolymer, *Colloids Surf., A*, 2020, **600**, 124866, DOI: 10.1016/J.COLSURFA.2020.124866.

19 X. Song, Y. Zhao, S. Hou, F. Xu, R. Zhao, J. He, Z. Cai, Y. Li and Q. Chen, Dual Agents Loaded PLGA Nanoparticles: Systematic Study of Particle Size and Drug Entrapment Efficiency, *Eur. J. Pharm. Biopharm.*, 2008, **69**(2), 445–453, DOI: 10.1016/J.EJPB.2008.01.013.

20 A. Budhian, S. J. Siegel and K. I. Winey, Haloperidol-Loaded PLGA Nanoparticles: Systematic Study of Particle Size and Drug Content, *Int. J. Pharm.*, 2007, **336**(2), 367–375, DOI: 10.1016/J.IJPHARM.2006.11.061.

21 T. Betancourt, B. Brown and L. Brannon-Peppas, Doxorubicin-Loaded PLGA Nanoparticles by Nanoprecipitation: Preparation, Characterization and *in vitro* Evaluation, *Nanomedicine*, 2007, **2**(2), 219–232, DOI: 10.2217/17435889.2.2.219.

22 C. Fonseca, S. Simões and R. Gaspar, Paclitaxel-Loaded PLGA Nanoparticles: Preparation, Physicochemical Characterization and *in vitro* Anti-Tumoral Activity, *J. Controlled Release*, 2002, **83**(2), 273–286, DOI: 10.1016/S0168-3659(02)00212-2.

23 K. Dillen, J. Vandervoort, G. Van Den Mooter, L. Verheyden and A. Ludwig, Factorial Design, Physicochemical Characterisation and Activity of Ciprofloxacin-PLGA Nanoparticles, *Int. J. Pharm.*, 2004, **275**(1–2), 171–187, DOI: 10.1016/J.IJPHARM.2004.01.033.

24 P. RS, K. Bomb, R. Srivastava and R. Bandyopadhyaya, Dual Drug Delivery of Curcumin and Niclosamide Using PLGA Nanoparticles for Improved Therapeutic Effect on Breast Cancer Cells, *J. Polym. Res.*, 2020, **27**(5), 133, DOI: 10.1007/s10965-020-02092-7.

25 A. Albisa, E. Piacentini, V. Sebastian, M. Arruebo, J. Santamaria and L. Giorno, Preparation of Drug-Loaded PLGA-PEG Nanoparticles by Membrane-Assisted Nanoprecipitation, *Pharm. Res.*, 2017, **34**(6), 1296–1308, DOI: 10.1007/s11095-017-2146-y.

26 K. Anwer, M. Mohammad, E. Ezzeldin, F. Fatima, A. Alalaiwe and M. Iqbal, Preparation of Sustained Release Apremilast-Loaded PLGA Nanoparticles: *in vitro* Characterization and *in vivo* Pharmacokinetic Study in Rats, *Int. J. Nanomed.*, 2019, **14**, 1587–1595, DOI: 10.2147/IJN.S195048.

27 R. Manchanda, A. Fernandez-Fernandez, A. Nagesetti and A. J. McGoron, Preparation and Characterization of a Polymeric (PLGA) Nanoparticulate Drug Delivery System with Simultaneous Incorporation of Chemotherapeutic and Thermo-Optical Agents, *Colloids Surf., B*, 2010, **75**(1), 260–267, DOI: 10.1016/J.COLSURFB.2009.08.043.

28 S. Lv, Y. Wu, K. Cai, H. He, Y. Li, M. Lan, X. Chen, J. Cheng and L. Yin, High Drug Loading and Sub-Quantitative Loading Efficiency of Polymeric Micelles Driven by Donor–Receptor Coordination Interactions, *J. Am. Chem. Soc.*, 2018, **140**(4), 1235–1238, DOI: 10.1021/jacs.7b12776.

29 Y. Shen, E. Jin, B. Zhang, C. J. Murphy, M. Sui, J. Zhao, J. Wang, J. Tang, M. Fan, E. Van Kirk and W. J. Murdoch, Prodrugs Forming High Drug Loading Multifunctional Nanocapsules for Intracellular Cancer Drug Delivery, *J. Am. Chem. Soc.*, 2010, **132**(12), 4259–4265, DOI: 10.1021/ja909475m.

30 K. Cai, X. He, Z. Song, Q. Yin, Y. Zhang, F. M. Uckun, C. Jiang and J. Cheng, Dimeric Drug Polymeric Nanoparticles with Exceptionally High Drug Loading and Quantitative Loading Efficiency, *J. Am. Chem. Soc.*, 2015, **137**(10), 3458–3461, DOI: 10.1021/ja513034e.

31 D. Li, G. Tang, H. Yao, Y. Zhu, C. Shi, Q. Fu, F. Yang and X. Wang, Formulation of PH-Responsive PEGylated Nanoparticles with High Drug Loading Capacity and Programmable Drug Release for Enhanced Antibacterial Activity, *Bioact. Mater.*, 2022, **16**, 47–56, DOI: 10.1016/J.BIOACTMAT.2022.02.018.

32 A. Sánchez, L. Vila-Jato and M. J. Alonso, Development of biodegradable microspheres and nanospheres for the controlled release of cyclosporin A, *Int. J. Pharm.*, 1993, **99**, 263–273, DOI: 10.1016/0378-5173(93)90369-Q.

33 S. Yee Win, M. Chavalitsarot, K. Eawsakul, T. Ongtanasup and N. Nasongkla, Encapsulation of Cyclosporine A-Loaded PLGA Nanospheres in Alginate Microbeads for Anti-Inflammatory Application, *ACS Omega*, 2024, **9**(6), 6901–6911, DOI: 10.1021/acsomega.3c08438.

34 S. Fredenberg, M. Wahlgren, M. Reslow and A. Axelsson, The Mechanisms of Drug Release in Poly(Lactic-*co*-Glycolic Acid)-Based Drug Delivery Systems—A Review, *Int. J. Pharm.*, 2011, **415**(1–2), 34–52, DOI: 10.1016/J.IJPHARM.2011.05.049.

35 K. I. Min, D. J. Im, H. J. Lee and D. P. Kim, Three-Dimensional Flash Flow Microreactor for Scale-Up Production of Monodisperse PEG-PLGA Nanoparticles, *Lab Chip*, 2014, **14**(20), 3987–3992, DOI: 10.1039/c4lc00700j.

36 J. Wang, W. Chen, J. Sun, C. Liu, Q. Yin, L. Zhang, Y. Xianyu, X. Shi, G. Hu and X. Jiang, A Microfluidic Tubing Method and Its Application for Controlled Synthesis of Polymeric Nanoparticles, *Lab Chip*, 2014, **14**(10), 1673–1677, DOI: 10.1039/c4lc00080c.

37 P. T. Le, S. H. An and H. H. Jeong, Microfluidic Tesla Mixer with 3D Obstructions to Exceptionally Improve the Curcumin Encapsulation of PLGA Nanoparticles, *Chem. Eng. J.*, 2024, **483**, 149377, DOI: 10.1016/J.CEJ.2024.149377.

38 Z. Liu, M. Yang, Q. Zhao, C. Yao and G. Chen, Scale-Up of Antisolvent Precipitation Process with Ultrasonic Microreactors: Cavitation Patterns, Mixing Characteristics and Application in Nanoparticle Manufacturing, *Chem. Eng. J.*, 2023, **475**, 146040, DOI: 10.1016/J.CEJ.2023.146040.

39 W. Li, Q. Chen, T. Baby, S. Jin, Y. Liu, G. Yang and C. X. Zhao, Insight into Drug Encapsulation in Polymeric Nanoparticles Using Microfluidic Nanoprecipitation, *Chem. Eng. Sci.*, 2021, **235**, 116468, DOI: 10.1016/J.CES.2021.116468.

40 X. Bai, S. Tang, S. Butterworth and A. Tirella, Design of PLGA Nanoparticles for Sustained Release of Hydroxyl-FK866 by Microfluidics, *Biomater. Adv.*, 2023, **154**, 213649, DOI: 10.1016/J.BIOADV.2023.213649.

41 C. B. Roces, D. Christensen and Y. Perrie, Translating the Fabrication of Protein-Loaded Poly(Lactic-*co*-Glycolic Acid) Nanoparticles from Bench to Scale-Independent Production Using Microfluidics, *Drug Delivery Transl. Res.*, 2020, **10**(3), 582–593, DOI: 10.1007/s13346-019-00699-y.
42 S. Wohlfart, S. Gelperina and J. Kreuter, Transport of Drugs across the Blood–Brain Barrier by Nanoparticles, *J. Controlled Release*, 2012, **161**(2), 264–273, DOI: 10.1016/J.JCONREL.2011.08.017.
43 D. Liu, B. Lin, W. Shao, Z. Zhu, T. Ji and C. Yang, *In vitro* and *in vivo* Studies on the Transport of PEGylated Silica Nanoparticles across the Blood–Brain Barrier, *ACS Appl. Mater. Interfaces*, 2014, **6**(3), 2131–2136, DOI: 10.1021/am405219u.
44 O. Betzer, M. Shilo, R. Opochinsky, E. Barnoy, M. Motiei, E. Okun, G. Yadid and R. Popovtzer, The Effect of Nanoparticle Size on the Ability to Cross the Blood–Brain Barrier: An *in vivo* Study, *Nanomedicine*, 2017, **12**(13), 1533–1546, DOI: 10.2217/nnm-2017-0022.
45 N. Tahir, A. Madni, W. Li, A. Correia, M. M. Khan, M. A. Rahim and H. A. Santos, Microfluidic Fabrication and Characterization of Sorafenib-Loaded Lipid-Polymer Hybrid Nanoparticles for Controlled Drug Delivery, *Int. J. Pharm.*, 2020, **581**, 15, DOI: 10.1016/j.ijpharm.2020.119275.
46 M. H. M. Leung and A. Q. Shen, Microfluidic Assisted Nanoprecipitation of PLGA Nanoparticles for Curcumin Delivery to Leukemia Jurkat Cells, *Langmuir*, 2018, **34**(13), 3961–3970, DOI: 10.1021/acs.langmuir.7b04335.
47 S. Rezvantalab and M. Keshavarz Moraveji, Microfluidic Assisted Synthesis of PLGA Drug Delivery Systems, *RSC Adv.*, 2019, 2055–2072, DOI: 10.1039/C8RA08972H.
48 I. O. De Solorzano, L. Uson, A. Larrea, M. Miana, V. Sebastian and M. Arruebo, Continuous Synthesis of Drug-Loaded Nanoparticles Using Microchannel Emulsification and Numerical Modeling: Effect of Passive Mixing, *Int. J. Nanomed.*, 2016, **11**, 3397–3416, DOI: 10.2147/IJN.S108812.
49 M. C. Operti, A. Bernhardt, V. Sincari, E. Jager, S. Grimm, A. Engel, M. Hruby, C. G. Figdor and O. Tagit, Industrial Scale Manufacturing and Downstream Processing of PLGA-Based Nanomedicines Suitable for Fully Continuous Operation, *Pharmaceutics*, 2022, **14**(2), 276, DOI: 10.3390/pharmaceutics14020276.
50 R. M. Mainardes and R. C. Evangelista, PLGA Nanoparticles Containing Praziquantel: Effect of Formulation Variables on Size Distribution, *Int. J. Pharm.*, 2005, **290**(1–2), 137–144, DOI: 10.1016/J.IJPHARM.2004.11.027.
51 J. Jaiswal, S. K. Gupta and J. Kreuter, Preparation of Biodegradable Cyclosporine Nanoparticles by High-Pressure Emulsification-Solvent Evaporation Process, *J. Controlled Release*, 2004, **96**(1), 169–178, DOI: 10.1016/J.JCONREL.2004.01.017.
52 N. Cherkasov, S. J. Adams, E. G. A. Bainbridge and J. A. M. Thornton, Continuous Stirred Tank Reactors in Fine Chemical Synthesis for Efficient Mixing, Solids-Handling, and Rapid Scale-Up, *React. Chem. Eng.*, 2022, 266–277, DOI: 10.1039/d2re00232a.
53 K. Y. Nandiwale, T. Hart, A. F. Zahrt, A. M. K. Nambiar, P. T. Mahesh, Y. Mo, M. J. Nieves-Remacha, M. D. Johnson, P. García-Losada, C. Mateos, J. A. Rincón and K. F. Jensen, Continuous Stirred-Tank Reactor Cascade Platform for Self-Optimization of Reactions Involving Solids, *React. Chem. Eng.*, 2022, **7**, 1315–1327, DOI: 10.1039/d2re00054g.
54 H. W. Chan, S. Chow, X. Zhang, P. C. L. Kwok and S. F. Chow, Role of Particle Size in Translational Research of Nanomedicines for Successful Drug Delivery: Discrepancies and Inadequacies, *J. Pharm. Sci.*, 2023, **112**(9), 2371–2384, DOI: 10.1016/J.XPHS.2023.07.002.
55 M. C. Operti, A. Bernhardt, S. Grimm, A. Engel, C. G. Figdor and O. Tagit, PLGA-Based Nanomedicines Manufacturing: Technologies Overview and Challenges in Industrial Scale-Up, *Int. J. Pharm.*, 2021, **605**(10), 120807, DOI: 10.1016/j.ijpharm.2021.120807.
56 N. Desai, Challenges in Development of Nanoparticle-Based Therapeutics, *AAPS J.*, 2012, 282–295, DOI: 10.1208/s12248-012-9339-4.
57 J. M. Metselaar and T. Lammers, Challenges in Nanomedicine Clinical Translation, *Drug Delivery Transl. Res.*, 2020, **10**(3), 721–725, DOI: 10.1007/s13346-020-00740-5.
58 S. Hua, M. B. C. de Matos, J. M. Metselaar and G. Storm, Current Trends and Challenges in the Clinical Translation of Nanoparticulate Nanomedicines: Pathways for Translational Development and Commercialization, *Front. Pharmacol.*, 2018, **9**, 790, DOI: 10.3389/fphar.2018.00790.
59 B. L. Banik, P. Fattahi and J. L. Brown, Polymeric Nanoparticles: The Future of Nanomedicine, *Wiley Interdiscip. Rev.:Nanomed. Nanobiotechnol.*, 2016, 271–299, DOI: 10.1002/wnan.1364.
60 T. L. Doane and C. Burda, The Unique Role of Nanoparticles in Nanomedicine: Imaging, Drug Delivery and Therapy, *Chem. Soc. Rev.*, 2012, **41**(7), 2885, DOI: 10.1039/c2cs15260f.
61 S. Zha, H. Liu, H. Li, H. Li, K.-L. Wong and A. Homayoun All, Functionalized Nanomaterials Capable of Crossing the Blood–Brain Barrier, *ACS Nano*, 2024, **18**(3), 1820–1845, DOI: 10.1021/acsnano.3c10674.
62 S. Mintova and J. Čejka, Micro/Mesoporous Composites, *Stud. Surf. Sci. Catal.*, 2007, **168**, 301, DOI: 10.1016/S0167-2991(07)80797-X.
63 A. P. Udepurkar, L. Mampaey, C. Clasen, V. Sebastián Cabeza and S. Kuhn, Microfluidic Synthesis of PLGA Nanoparticles Enabled by an Ultrasonic Microreactor, *React. Chem. Eng.*, 2024, **9**, 2208–2217, DOI: 10.1039/d4re00107a.
64 *ICH Guideline Q3C (R8) on Impurities: Guideline for Residual Solvents*, European Medicines Agency, 2022, pp. , pp. 1–51.
65 R. Arshady, Preparation of biodegradable microspheres and microcapsules: 2. Polyactides and related polyesters, *J. Controlled Release*, 1991, **17**, 1–21, DOI: 10.1016/0168-3659(91)90126-X.
66 J. Wang, and S. P. Schwendeman, *Mechanisms of Solvent Evaporation Encapsulation Processes: Prediction of Solvent Evaporation Rate*, 1999, DOI: 10.1021/js980169z.
67 H. Katou, A. J. Wandrey and B. Gander, Kinetics of Solvent Extraction/Evaporation Process for PLGA Microparticle

Fabrication, *Int. J. Pharm.*, 2008, **364**(1), 45–53, DOI: 10.1016/J.IJPHARM.2008.08.015.

68 G. Liu and K. McEnnis, Glass Transition Temperature of PLGA Particles and the Influence on Drug Delivery Applications, *Polymers*, 2022, **14**(5), 993, DOI: 10.3390/polym14050993.

69 K. Park, A. Otte, F. Sharifi, J. Garner, S. Skidmore, H. Park, Y. K. Jhon, B. Qin and Y. Wang, Potential Roles of the Glass Transition Temperature of PLGA Microparticles in Drug Release Kinetics, *Mol. Pharmaceutics*, 2021, 18–32, DOI: 10.1021/acs.molpharmaceut.0c01089.

70 P. I. P. Park and S. Jonnalagadda, Predictors of Glass Transition in the Biodegradable Polylactide and Poly-Lactide-*co*-Glycolide Polymers, *J. Appl. Polym. Sci.*, 2006, **100**(3), 1983–1987, DOI: 10.1002/app.22135.

71 S. A. Abouelmagd, B. Sun, A. C. Chang, Y. J. Ku and Y. Yeo, Release Kinetics Study of Poorly Water-Soluble Drugs from Nanoparticles: Are We Doing It Right?, *Mol. Pharmaceutics*, 2015, **12**(3), 997–1003, DOI: 10.1021/mp500817h.

72 L. Tang, J. Azzi, M. Kwon, M. Mounayar, R. Tong, Q. Yin, R. Moore, N. Skartsis, T. M. Fan, R. Abdi and J. Cheng, Immunosuppressive Activity of Size-Controlled PEG-PLGA Nanoparticles Containing Encapsulated Cyclosporine A, *J. Transplant.*, 2012, **2012**, 1–9, DOI: 10.1155/2012/896141.

73 U. S. Food and Drug Administration, *Advancement of Emerging Technology Applications for Pharmaceutical Innovation and Modernization Guidance for Industry*, 2017, http://www.fda.gov/Drugs/GuidanceComplianceRegulatoryInformation/Guidances/default.htm.

